J. Cent. South Univ. (2015) 22: 4329−4336
DOI: 10.1007/s11771-015-2981-0

Springer

Physical modelling of pipe piles under oblique pullout loads using transparent soil and particle image velocimetry

CAO Zhao-hu(曹兆虎)[1], LIU Han-long(刘汉龙)[1, 2], KONG Gang-qiang(孔纲强)[1], ZHOU Hang(周航)[1]

1. College of Civil and Transportation Engineering, Hohai University, Nanjing 210098, China;
2. Key Laboratory of New Technology for Construction of Cities in Mountain Area, Chongqing University, Chongqing 400045, China

Abstract: A small-scale physical modelling method was developed to investigate the pile bearing capacity and the soil displacement around the pile using transparent soil and particle image velocimetry (PIV) technique. Transparent sand was made of baked quartz and a pore fluid with a matching refractive index. The physical modelling system consists of a loading system, a laser light, a CCD camera, an optical platform and a computer for image analyzing. A distinctive laser speckle was generated by the interaction between the laser light and transparent soil. Two laser speckle images before and after deformation were used to calculate the soil displacement field using PIV. Two pipe piles with different diameters under oblique pullout loads at angles of 0°, 30°, 45°, 60° and 90° were used in tests. The load−displacement response, oblique pullout ultimate resistances and soil displacement fields were then studied. The test results show that the developed physical modelling method and transparent soil are suitable for pile−soil interaction problems. The soil displacements around the pipe piles will improve the understanding on the capacity of pipe piles under oblique pullout loads.

Key words: pipe piles; transparent soil; particle image velocimetry (PIV); displacement fields; oblique pullout loads

1 Introduction

Pipe piles are widely used for foundations in construction both on land and offshore. For most time, pipe piles are subjected to vertical and lateral combined loads [1]. The problem of single pile or pile group under oblique loads had been investigated by some researchers [2−4]. However, all these studies mentioned above focused only on the loading capacity where limited information was available on soil deformation around the pile.

Particle image velocimetry (PIV) is an optical method to measure instantaneous flow displacement vectors by tracking seeded particle movement which now has been widely used in geotechnical engineering to study soil deformation problems. WHITE and BOLTON [5] used this technique to study displacement and strain paths during plane-strain pile installation in sand. LIU et al [6] investigated sand deformation around a laterally loaded pile using PIV. Afterward, YUAN et al [7] obtained 3D soil deformation around a laterally loaded pile in sand using stereo-PIV.

In traditional field and laboratory tests it is naturally difficult to measure displacements inside soil mass. In recent years, the development of transparent soil manufactured by ISKNADER et al [8−9] has made it possible to see movement inside a soil body in laboratory tests. LEHANE and GILL [10] used transparent soil and obtained the displacement path of black spherical beads embedded in the transparent soil during the model pile installation. Subsequently, NI et al [11] combined the use of transparent soil and PIV technique and observed the whole deformation field within the soil body during the model pile installation. The results showed that such a method could be capable for investigating more complicated geotechnical process at laboratory scale.

Hence, based on transparent soil and PIV technique, a physical modelling system consisting of a loading system, a laser light, a CCD camera, an optical platform and a computer was developed in this study. Two pipe piles with different diameters under oblique pullout loads at angles, α=0°, 30°, 45°, 60° and 90° were conducted in transparent sand. The load−displacement response, oblique pullout ultimate resistances, and soil displacements fields were obtained through the model test. The test results demonstrated that the whole developed system could be capable for more advanced

Foundation item: Project(51478165) supported by the National Natural Science Foundation of China; Project(2013B31814, 2014B07214) supported by the Fundamental Research Funds for the Central Universities, China
Received date: 2014−10−08; **Accepted date:** 2015−03−19
Corresponding author: KONG Gang-qiang, Associate Professor, PhD; Tel: +86−25−83787772; E-mail: gqkong1@163.com

geotechnical laboratory testing.

2 Model test description

2.1 Model test set-up

The model test set-up, as shown in Fig. 1, consists of a loading system, a laser light, a CCD camera, an optical platform, and a computer for image processing. The loading system was composed of a sliding bracket, two movable pulleys and several loads. The laser light, manufactured by Nanjing Laichuang Laser Technology Co., Ltd., China, could produce a maximum output power of 2 W. A line generator lens was utilized to create a laser light sheet to slice the transparent soil sample. The CCD camera with a resolution of 1280 × 960 pixels was set approximately 500 mm away from the laser sheet with its optical axis perpendicular to the laser sheet plane. It was controlled by the PC through the software "MV-Capture" provided by the camera manufacturer. A macro zoom lens was used to adjust the size of the captured area. The images (before and after deformation) could be captured and stored in the computer. The optical platform could provide a secure and stable platform for the test process, and all the devices can be fixed on this platform by bolts.

A Plexiglas square box with a thickness of 5 mm and inner dimensions of 120 mm×120 mm×250 mm (L×W×H) was used in this investigation, and it was fixed on the optical platform by bolts. Two model pipe piles with a same wall thickness of 3 mm and different outside diameters, 15 mm for Pile A and 20 mm for Pile B, were used in the tests. Both model piles were made of Plexiglas material. The model piles were embedded approximately 100 mm in the transparent sand. The pile was connected to the loading frame through a string at a loading point, which was about 10 mm above the sample height. During the tests the pile was subjected to oblique pullout loads at angles, α=0°, 30°, 45°, 60° and 90° with the vertical axis of the pile.

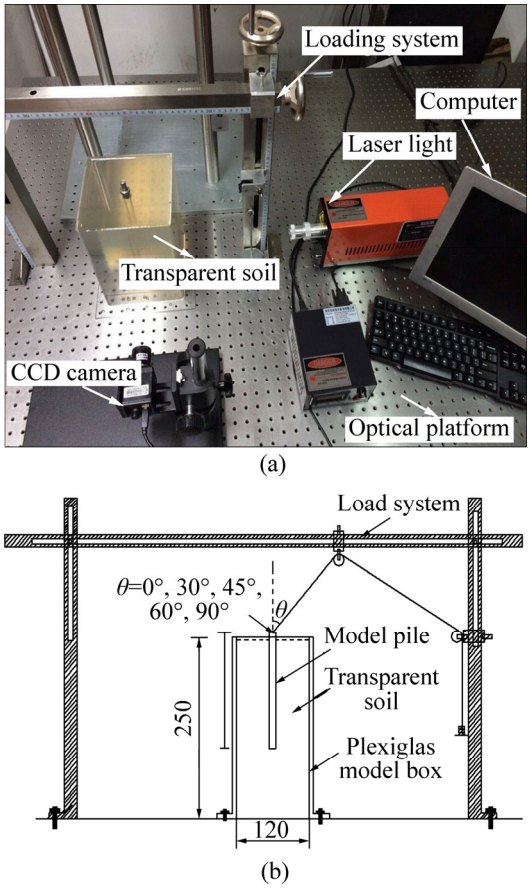

Fig. 1 Physical photo (a) and schematic diagram (b) of model test set-up (Unit: mm)

2.2 Sample preparation

The transparent soils were manufactured by transparent materials and a pore fluid with a matching refractive index. In this work, baked quartz, which was manufactured by Xuzhou Xinyi Wanhe Minerals Co., Ltd. in China, was chosen for transparent soil material. The size of the used baked quartz ranges from 0.5 mm to 1.0 mm, and its physical photo and microstructure with 80 times magnification are shown in Figs. 2(a) and (b), respectively. The specific gravity of the baked quartz was 2.186 with a uniformity coefficient C_u of 1.83 and a gradation coefficient C_c of 1.00. The minimum dry density, ρ_{min}, and maximum dry density, ρ_{max}, were 0.970 g/cm^3 and 1.274 g/cm^3, respectively. The refractive index of the baked quartz was 1.4586. The matching pore fluid was 25:75 blends by mass of colorless N-Paraffin C 12 and Technical White Oil 15 [12]. The refractive index of the pore fluid was 1.4586 at 24 °C. The engineering properties of the transparent sand made by baked quartz were studied by KONG et al [13]. The friction angles of the transparent sand from triaxial tests with 30% and 70% relative densities were 37.1° and 39.4°, respectively.

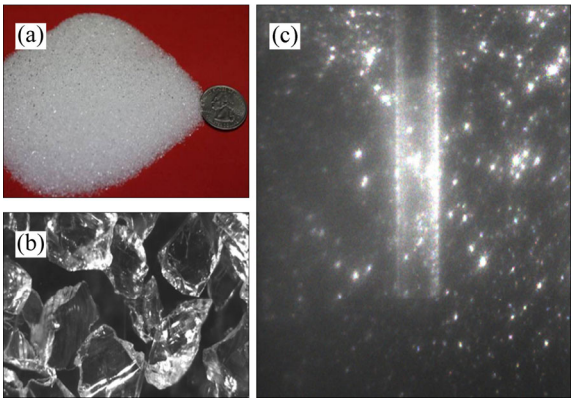

Fig. 2 Physical photos of transparent sand manufactured by baked quartz (a, b) and its speckle pattern (c)

Before mixing the soil sample, it was important to thoroughly clean and dry all beakers, dishes and boxers

used in the sample preparation process [14]. After baked quartz was immersed in the pore fluid, a whisk was used to stir the slurry to ensure thorough mixing. Afterward, a vacuum was applied to de-air the mix. Finally, the sample was packed into the Plexiglas box. In these tests, nearly 50% relative density of soil sample was modeled. The model pile was manually driven into the soil sample to the desired depth and the string was attached to the pile. The tests were performed in a darkroom and the distinctive speckle pattern between the transparent sand and the laser light sheet with the model pile is shown in Fig. 2(c).

2.3 Particle image velocimetry

PIV technique was a classical pattern recognition technique based on using the correlation function to locate the best matching position of two images. For displacements measurements with the PIV, the whole image area was divided into many smaller interrogated windows. For each of these interrogation windows, the images before and after each decrement of load pressure were correlated to produce an average particle displacement vector. Doing this for all interrogation regions could produce a vector map of average particle displacements. The discrete form of standard cross-correlation function is as follows:

$$C(\Delta x,\Delta y)=\frac{1}{MN}\sum_{m=0}^{M-1}\sum_{n=0}^{N-1}f(m,n)g(m+\Delta x,n+\Delta y) \quad (1)$$

where M and N are the dimensions of the interrogated images; f and g are the grayscale intensities of two images being interrogated. SADEK et al [15] studied the accuracy of PIV application in transparent soil models. The results indicated that the calculated deformation using the developed system has an error on the order 0.1 pixel which is capable for image processing in such model tests. More details of the accuracy and correlation function of the PIV technique can be found in Refs. [15−16].

It is also noticeable that the parallax effect observed by WHITE et al [17] was deemed negligible since in this work the camera was positioned perpendicular and centered to the plane of measurement [18].

3 Results and discussions

3.1 Load−displacement response

The oblique pullout load versus vertical or lateral displacement curves for the model pipe piles with different outside diameters (D=15 mm and 20 mm) are shown in Fig. 3. Figures 3(a) and (c) show the oblique pullout load versus vertical displacement of the model

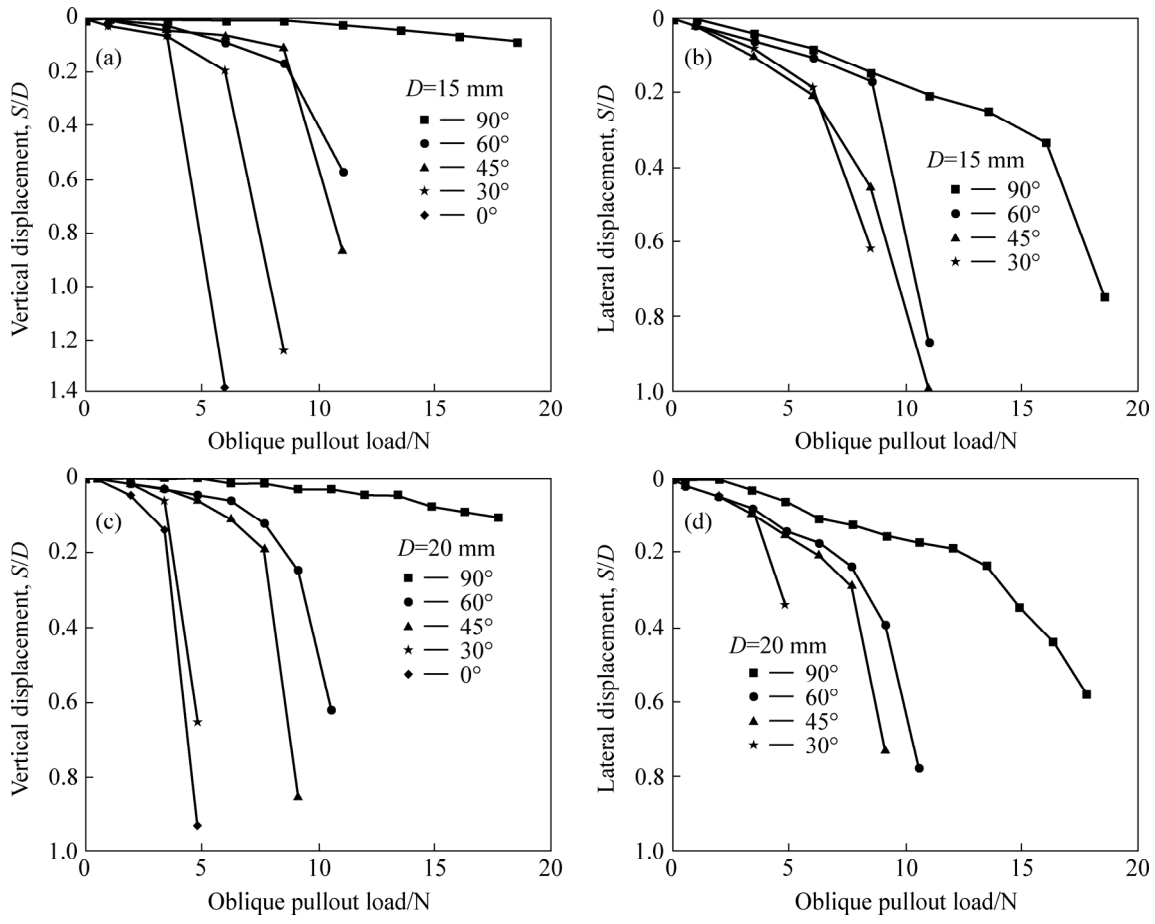

Fig. 3 Curves of oblique pullout load versus axial (vertical (a, c) or lateral (b, d)) displacement for model piles

piles. Figures 3(b) and (d) show the oblique pullout load versus lateral displacement of the model piles, respectively. In general, all the load−displacement curves are non-linear. In Fig. 3 it is worthy noticing that the model piles have the minimum lateral or vertical displacements when they were subjected to the oblique pullout loads at angle of 90°, except for the fact that when the model piles were subjected to the oblique load at angle of 0°, they have no lateral but vertical displacements. It is also clear that when the model piles were subjected to the oblique pullout loads at angle of 0°, they have the maximum vertical displacements. From Fig. 3, it is shown that piles under pure lateral load (α=90°) could have the maximum bearing capacity and piles under pure vertical pullout load (α=0°) would have the minimum bearing capacity.

The oblique pullout load versus vertical or lateral displacement curves obtained by KRISHNA and PATRA [2], and PATRA and PISE [3] are shown in Fig. 4 for comparative analysis. Figures 4(a), (c), (e), (g) and (i) show the curves of the oblique pullout load versus vertical displacement of the piles under oblique pullout load at different angles (α=90°, 60°, 45°, 30°, and 0°). Figures 4(b), (d), (f) and (h) show the curves of the oblique pullout load versus lateral displacement of the piles under oblique pullout load at different angles (α=90°, 60°, 45°, and 30°). The load−displacement curves obtained in this work are much steeper than those obtained in the previous works. This is mainly due to the small scale of the model piles used in this study. In Fig. 4 it is obvious that when the piles were subjected to the same oblique pullout load, the mobilized vertical or lateral displacement decreases with increasing pile diameter regardless of the oblique pullout load angles.

3.2 Ultimate bearing capacity

The mode of failure is determined from load−displacement curves. In the case of the piles under pure lateral load (α=90°), the failure mode is lateral or normal failure; the piles under pure vertical pullout load (α=0°), the failure mode is axial failure. Similarly, when the piles were subjected to the oblique pullout loads, the minimum failure load obtained from displacement curves could be taken as the ultimate failure load. And the failure mode could be taken as the displacement corresponding to the minimum failure load. For example, when α=60°, the displacement corresponding to the minimum failure load is the lateral displacement; hence, the failure mode for this case is lateral failure. In this work, the ultimate failure load has been found out where a large displacement occurs for a small increment in the applied load as KRISHNA and PATRA [2], PATRA and PISE [3] did in the previous works. It is the point where the curve exhibits a peak or the displacement maintains a continuous increase with no further increase in the oblique pullout load. For some cases where the peak points were not obvious, the ratio of soil displacement to pile diameter was selected to determine the ultimate bearing capacity. The ultimate bearing capacity of the piles under the oblique pullout loads (α=90°, 60°, 45°, 30°, and 0°) are listed in Table 1. For example, when α=60°, the ultimate bearing capacities of Pile A and Pile B equal 8.5 N and 12.4 N, respectively. It is clear that the bearing capacity of Pile A is smaller than that of Pile B when α is the same. As expected, the piles under pure lateral load (α=90°) have the the maximum bearing capacity and piles under pure vertical pullout load (α=0°) have the minimum bearing capacity except one case done by PATRA and PISE [3] because of the rough pile surfaces.

3.3 Soil displacement fields under failure load

In order to improve the interpretation and understanding of pile−soil interaction problems, soil displacements around the model piles were studied. Take α=90° for example, the accumulated displacement vectors when the load increased from 0 N to 16.0 N for Pile A and from 0 N to 23.5 N for Pile B were calculated using PIVview2C and then shown in Figs. 5(a) and (b), respectively. It is clear that the displacement vectors patterns around the two piles are similar, indicating that the failure modes are the same. In order to show clearly soil movement, the displacement contours were plotted in Fig. 6. Figures 6(a) and (b) show the lateral displacement contours around the model piles while Figs. 6(c) and (d) present the vertical displacement contours around the piles. From Fig. 6 we could see that for both the piles under pure lateral failure load, the soil displacements around the piles became zero at 70%−80% of the pile imbedded depth which consists with the results investigated by ZHOU et al [19].

3.4 Soil displacement fields under working load

For seeking the soil displacement fields under the working load, the piles under α=60° and 8.5 N oblique pullout load were chosen for analysis. The accumulated displacement vectors around Pile A and Pile B as the oblique pullout load increased from 0 N to 8.5 N are shown in Figs. 7(a) and (b), respectively. In Fig. 7 it is clear that the displacement vectors patterns around the piles are similar. To display the components of the displacements fields, the displacement contours were also produced. The lateral displacement contours around the piles are shown in Figs. 8(a) and (b), respectively.

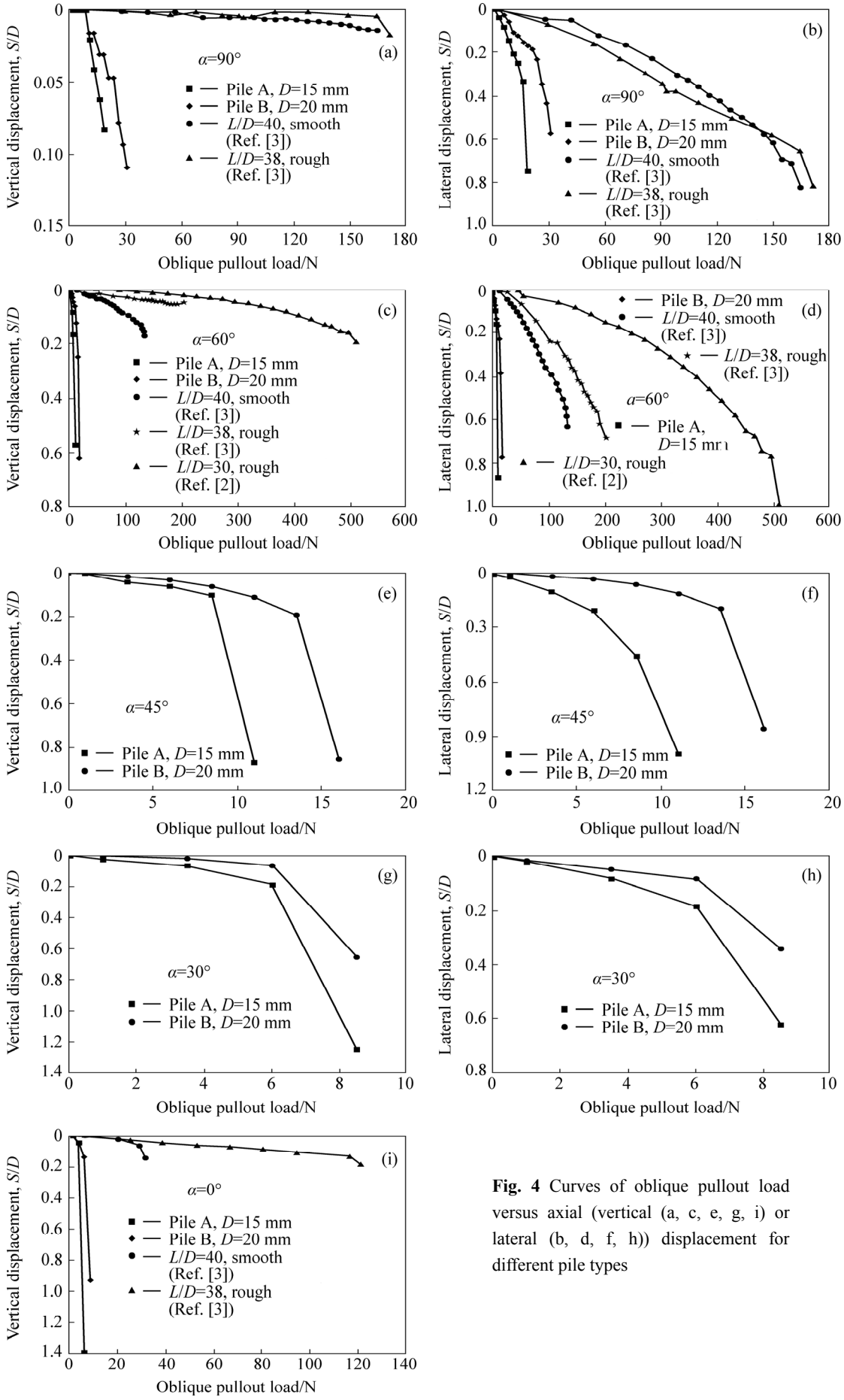

Fig. 4 Curves of oblique pullout load versus axial (vertical (a, c, e, g, i) or lateral (b, d, f, h)) displacement for different pile types

Table 1 Ultimate bearing capacity (Q_{ult}) of piles under oblique pullout loads (Unit: N)

Item	Type	Q_{ult}/N				
		α=0°	α=30°	α=45°	α=60°	α=90°
Pile A	D=15 mm	3.8	5.8	6.1	8.5	10.6
Pile B	D=20 mm	6.3	6.6	10.8	12.4	22.1
Ref. [3]	Smooth L/D=40	20.2	27.9	−	130.7	149.6
	Rough L/D=38	116.4	204.6	−	186.9	164.3
Ref. [2]	L/D=30	204.2	364.4	−	330.0	394.4
	L/D=20	118.5	156.9	−	161.8	232.2

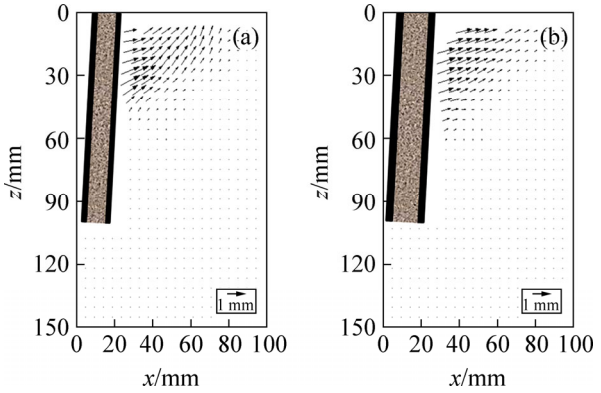

Fig. 5 Displacement vectors around piles A (a) and B (b) under the failure load

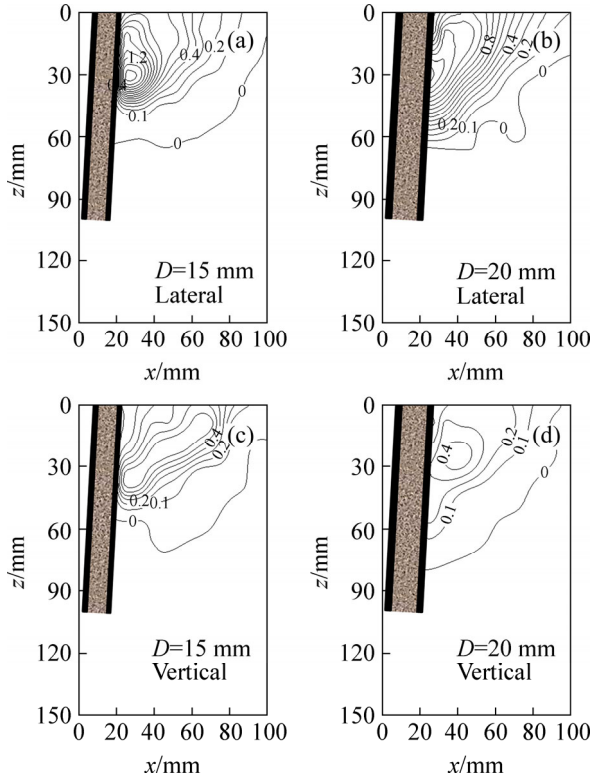

Fig. 6 Displacement contours (lateral (a, b) and vertical (c, d)) around piles under failure load

The vertical displacement contours around the piles are presented in Fig. 8(c) and Fig. 8(d), respectively. In

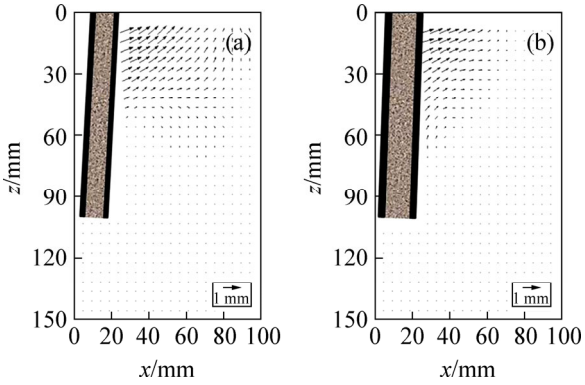

Fig. 7 Displacement vectors around piles A (a) and B (b) under working load

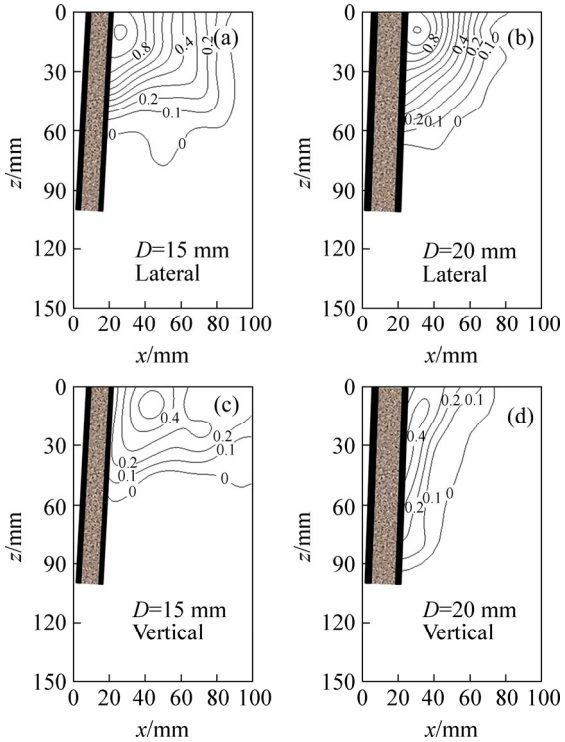

Fig. 8 Displacement contours (lateral (a, b) and vertical (c, d)) around piles under working load

Fig. 8 it is obvious that the soil displacements around Pile B are smaller than those around Pile A because of its larger diameter. It is also clear the influenced area around Pile B is smaller than that around Pile A.

In order to see the soil displacements around the pile under the oblique pullout load at different angles, Pile B under the working load of 6.0 N was chosen for analysis. The soil displacement fields around Pile B under the oblique pullout load at different angles (α=90°, 60°, 45°, 30°, and 0°) are displayed in the form of vector quiver plots in Fig. 9. To display the lateral and vertical displacement fields, contour plots were also produced. These are shown in Fig. 10. It can be seen that the displacement fields of Pile B under the oblique pullout load at different angles have some noticeable differences.

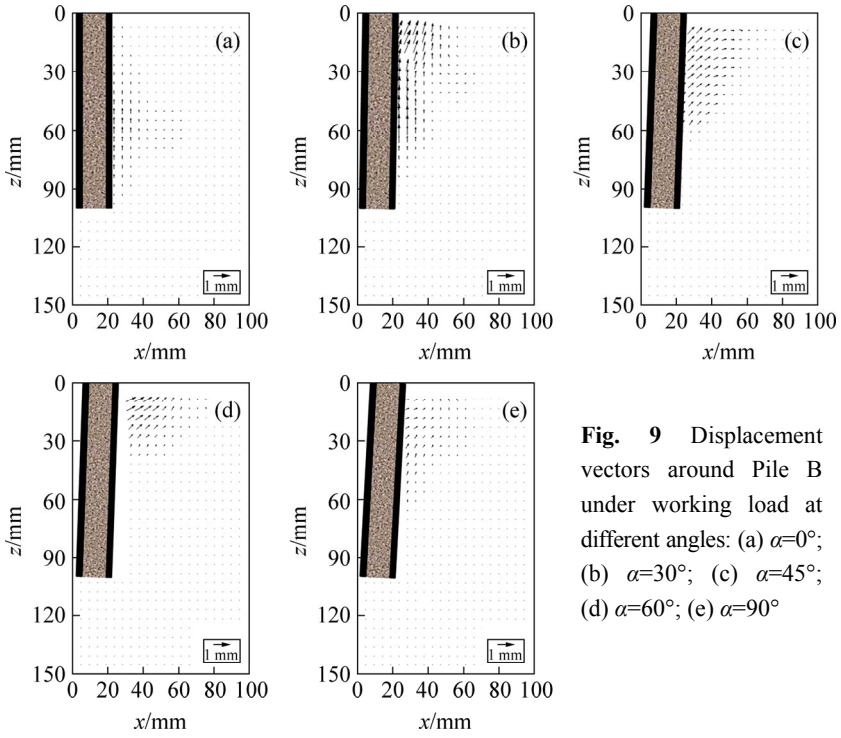

Fig. 9 Displacement vectors around Pile B under working load at different angles: (a) α=0°; (b) α=30°; (c) α=45°; (d) α=60°; (e) α=90°

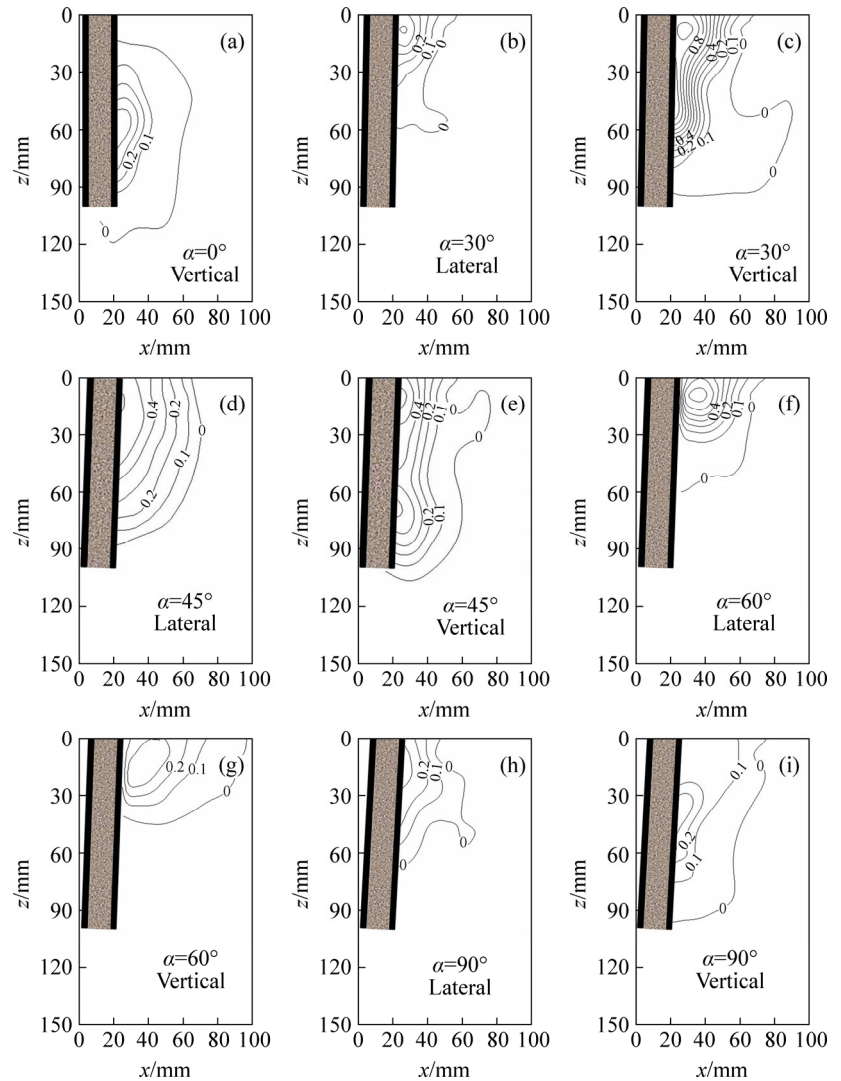

Fig. 10 Displacement contours (lateral or vertical) around Pile B under working load at different angles

When α=0°, the soils particles around the pile move upwards. And when α=30°, the vertical displacements are bigger than the lateral displacements; however, for α=90°, 60°, 45°, the vertical displacements and the lateral displacements are more or less the same.

4 Conclusions

1) A physical modelling method is developed, combining the use of transparent soil and PIV technique to measure internal soil deformation caused by pile moving under the oblique pullout loads. The visualization of spatial deformation inside soil masses will improve the understanding on the capacity of the piles under the oblique pullout loads.

2) Test results show that the developed physical modelling system and transparent soil are suitable for studying the problems of pile−soil interaction under the oblique pullout loads. It could have a wider application in geotechnical engineering.

3) The piles under pure lateral load (α=90°) could have the maximum bearing capacity and the piles under pure vertical pullout load (α=0°) have the minimum bearing capacity if the pile surfaces are smooth.

4) When the piles are subjected to pure vertical pullout load (α=0°), the soil displacement vectors and displacement contours around the piles are quite different from those around the piles which are under the oblique pullout load at α=30°, 45°, 60° and 90°. This may indicate the difference between the failure moods.

5) However, there are still some limitations in this study. The same problem with other physical models is that the tests are performed on a scaled model at gravity condition in this study; hence, transparent soil used in centrifuge physical model tests will be one of important research directions.

Acknowledgements

The authors are grateful to Associate Professor Jinyuan LIU at Ryerson University for his great help.

References

[1] CHEN J Y, GILBERT R B, PUSKAR F J, VERRET S. Case study of offshore pile system failure in hurricane ike [J]. Journal of Geotechnical and Geoenvironmental Engineering, 2013, 139(10): 1699−1708.

[2] KRISHNA B, PATRA N R. Effect of compressive load on oblique pull-out capacity of model piles in sand [J]. Geotechnical and Geological Engineering, 2006, 24(3): 593−614.

[3] PATRA N R, PISE P J. Model pile groups under oblique pullout loads — An investigation [J]. Geotechnical and Geological Engineering, 2006, 24(2): 265−282.

[4] JOHNSON K, LEMCKE P, KARUNASENA W, SIVAKUGAN N. Modelling the load–deformation response of deep foundations under oblique loading [J]. Environmental Modelling & Software, 2006, 21(9): 1375−1380.

[5] WHITE D J, BOLTON M D. Displacement and strain paths during plane-strain model pile installation in sand [J]. Geotechnique, 2004, 54(6): 375−397.

[6] LIU J, YUAN B X, MAI V T, DIMAANO R. Optical measurement of sand deformation around a laterally loaded pile [J]. Journal of Testing and Evaluation, 2011, 39(5): 1−6.

[7] YUAN Bing-xiang, CHEN Wen-wu, JIANG Tong, WANG Yi-xian, CHEN Ke-ping. Stereo particle image velocimetry measurement of 3D soil deformation around laterally loaded pile in sand [J]. Journal of Central South University, 2013, 20(3): 791−798.

[8] ISKANDER M, SADEK S, LIU J. Optical measurement of deformation using transparent silica gel to model sand [J]. International Journal of Physical Modelling in Geotechnics, 2002, 2(4): 13−26.

[9] ISKNADER M, LIU J, SADEK S. Transparent amorphous silica to model clay [J]. Journal of Geotechnical and Geoenvironmental Engineering, 2002, 128(3): 262−273.

[10] LEHANE B M, GILL D R. Displacement fields induced by penetrometer installation in an artificial soil [J]. International Journal of Physical Modelling in Geotechnics, 2004, 4(1): 25−36.

[11] NI Q, HIRD C C, GUYMER I. Physical modelling of pile penetration in clay using transparent soil and particle image velocimetry [J]. Geotechnique, 2010, 60(2): 121−132.

[12] ZHAO H, GE L, LUNA R. Low viscosity pore fluid to manufacture transparent soil [J]. Geotechnical Testing Journal, 2010, 33(6): 1−6.

[13] KONG Gang-qiang, LIU Lu, LIU Han-long, ZHOU Hang. Triaxial tests on deformation characteristics of transparent glass sand [J]. Chinese Journal of Geotechnical Engineering, 2013, 35(6): 1140−1146. (in Chinese)

[14] WELKER A L, BOWDERS J J, GILBERT R B. Applied research using a transparent material with hydraulic properties similar to soil [J]. Geotechnical Testing Journal, 1999, 22(3): 266−270.

[15] SADEK S, ISKANDER M, LIU J. Accuracy of digital image correlation for measuring deformation in transparent media [J]. Journal of Computing in Civil Engineering, 2003, 17(2): 88−96.

[16] LIU J, ISKANDER M. Adaptive cross correlation for imaging displacements in soils [J]. Journal of Computing in Civil Engineering, 2004, 18(1): 46−57.

[17] WHITE D J, TAKE W A, BOLTON M D. Soil deformation measurement using particle image velocimetry (PIV) and photogrammetry [J]. Geotechnique, 2003, 53(7): 619−631.

[18] AHMED M, ISKANDER M. Analysis of tunneling-induced ground movements using transparent soil models [J]. Journal of Geotechnical and Geoenvironmental Engineering, 2011, 137(5): 525−535.

[19] ZHOU Jian, ZHANG Gang, ZENG Qing-you. Model tests and PFC^{2D} numerical analysis of active laterally loaded piles [J]. Chinese Journal of Geotechnical Engineering, 2007, 29(5): 650−656. (in Chinese)

(Edited by YANG Hua)